Pure

Syddansk Universitet

Directional coupling in channel plasmon-polariton waveguides

Zenin, Volodymyr; Volkov, Valentyn S.; Han, Zhanghua; Bozhevolnyi, Sergey I.; Devaux, Eloïse; Ebbesen, Thomas W.

Published in:
Optics Express

Publication date:
2012

Document Version
Final published version

Link to publication

Citation for pulished version (APA):
Zenin, V., Volkov, V. S., Han, Z., Bozhevolnyi, S. I., Devaux, E., & Ebbesen, T. W. (2012). Directional coupling in channel plasmon-polariton waveguides. Optics Express, 20(6), 6124-6134.

General rights
Copyright and moral rights for the publications made accessible in the public portal are retained by the authors and/or other copyright owners and it is a condition of accessing publications that users recognise and abide by the legal requirements associated with these rights.

- Users may download and print one copy of any publication from the public portal for the purpose of private study or research.
- You may not further distribute the material or use it for any profit-making activity or commercial gain
- You may freely distribute the URL identifying the publication in the public portal ?

Take down policy
If you believe that this document breaches copyright please contact us providing details, and we will remove access to the work immediately and investigate your claim.

Download date: 17. jan.. 2017

Directional coupling in channel plasmon-polariton waveguides

Vladimir A. Zenin,[1,2,*] Valentyn S. Volkov,[1] Zhanghua Han,[1] Sergey I. Bozhevolnyi,[1] Eloïse Devaux,[3] and Thomas W. Ebbesen[3]

[1]*Institute of Technology and Innovation, University of Southern Denmark, Niels Bohrs Allé 1, DK-5230 Odense M, Denmark*

[2]*Laboratory of Nanooptics and Femtosecond Electronics, Moscow Institute of Physics and Technology (State University), Institutsky Lane 9, 141700 Dolgoprudny, Russia*

[3]*Laboratoire des Nanostructures, ISIS, Université de Strasbourg, CNRS (UMR7006), 8 allée Gaspard Monge, 67000 Strasbourg, France*

[*]*zenin@iti.sdu.dk*

Abstract: We investigate directional couplers (DCs) formed by channel plasmon-polariton (CPP) waveguides (CPPWs). DCs comprising 5-μm-offset S-bends and 40-μm-long parallel CPPWs with different separations (0.08, 0.25, 0.5 and 2 μm) between V-groove channels are fabricated by using a focused ion-beam (FIB) technique in a 2-μm-thick gold film and characterized at telecom wavelengths (1425-1630 nm) with near-field optical microscopy. Experimental results reveal strong coupling, resulting in approximately equal power splitting between DC-CPPWs, for small CPPW separations (0.08 and 0.25 μm). The coupling gradually deteriorates with the increase of separation between V-grooves and practically vanishes for the separation of 2 μm. The DC-CPPW characteristics observed are found in good agreement with finite-element method (implemented in COMSOL) simulations.

©2012 Optical Society of America

OCIS codes: (230.7380) Waveguides, channeled; (240.6680) Surface plasmons.

References and links

1. V. M. Agranovich and D. L. Mills, eds., *Surface Polaritons* (North-Holland, 1982).
2. H. Raether, *Surface Plasmons* (Springer-Verlag, 1988).
3. N. E. Glass, A. A. Maradudin, and V. Celli, "Theory of surface-polariton resonances and field enhancements in light scattering from bigratings," J. Opt. Soc. Am. **73**(10), 1240–1248 (1983).
4. J. M. Pitarke, V. M. Silkin, E. V. Chulkov, and P. M. Echenique, "Theory of surface plasmons and surface-plasmon polaritons," Rep. Prog. Phys. **70**(1), 1–87 (2007).
5. S. I. Bozhevolnyi and F. Pudonin, "Two-dimensional micro-optics of surface plasmons," Phys. Rev. Lett. **78**(14), 2823–2826 (1997).
6. T. W. Ebbesen, H. J. Lezec, H. F. Ghaemi, T. Thio, and P. A. Wolff, "Extraordinary optical transmission through sub-wavelength hole arrays," Nature **391**(6668), 667–669 (1998).
7. J. K. Lim, K. Imura, T. Nagahara, S. K. Kim, and H. Okamoto, "Imaging and dispersion relations of surface plasmon modes in silver nanorods by near-field spectroscopy," Chem. Phys. Lett. **412**(1-3), 41–45 (2005).
8. T. W. Ebbesen, C. Genet, and S. I. Bozhevolnyi, "Surface-plasmon circuitry," Phys. Today **61**(5), 44–50 (2008).
9. D. K. Gramotnev and S. I. Bozhevolnyi, "Plasmonics beyond the diffraction limit," Nat. Photonics **4**(2), 83–91 (2010).
10. J. A. Conway, S. Sahni, and T. Szkopek, "Plasmonic interconnects versus conventional interconnects: a comparison of latency, crosstalk and energy costs," Opt. Express **15**(8), 4474–4484 (2007).
11. H. Ditlbacher, A. Hohenau, D. Wagner, U. Kreibig, M. Rogers, F. Hofer, F. R. Aussenegg, and J. R. Krenn, "Silver nanowires as surface plasmon resonators," Phys. Rev. Lett. **95**(25), 257403 (2005).
12. M. L. Brongersma, J. W. Hartman, and H. A. Atwater, "Electromagnetic energy transfer and switching in nanoparticle chain arrays below the diffraction limit," Phys. Rev. B **62**(24), 16356–16359 (2000).
13. S. A. Maier, M. L. Brongersma, P. G. Kik, and H. A. Atwater, "Observation of near-field coupling in metal nanoparticle chains using far-field polarization spectroscopy," Phys. Rev. B **65**(19), 193408 (2002).
14. J. R. Krenn and J. C. Weeber, "Surface plasmon polaritons in metal stripes and wires," Philos. Trans. A Math. Phys. Eng. Sci. **362**(1817), 739–756 (2004).

#162315 - $15.00 USD Received 31 Jan 2012; revised 24 Feb 2012; accepted 24 Feb 2012; published 29 Feb 2012
(C) 2012 OSA

15. A. Boltasseva, T. Nikolajsen, K. Leosson, K. Kjaer, M. S. Larsen, and S. I. Bozhevolnyi, "Integrated optical components utilizing long-range surface plasmon polaritons," J. Lightwave Technol. **23**(1), 413–422 (2005).
16. J. Gosciniak, V. S. Volkov, S. I. Bozhevolnyi, L. Markey, S. Massenot, and A. Dereux, "Fiber-coupled dielectric-loaded plasmonic waveguides," Opt. Express **18**(5), 5314–5319 (2010).
17. K. Tanaka, M. Tanaka, and T. Sugiyama, "Simulation of practical nanometric optical circuits based on surface plasmon polariton gap waveguides," Opt. Express **13**(1), 256–266 (2005).
18. I. V. Novikov and A. A. Maradudin, "Channel polaritons," Phys. Rev. B **66**(3), 035403 (2002).
19. S. I. Bozhevolnyi, V. S. Volkov, E. Devaux, and T. W. Ebbesen, "Channel plasmon-polariton guiding by subwavelength metal grooves," Phys. Rev. Lett. **95**(4), 046802 (2005).
20. V. S. Volkov, S. I. Bozhevolnyi, E. Devaux, and T. W. Ebbesen, "Bend loss for channel plasmon polaritons," Appl. Phys. Lett. **89**(14), 143108 (2006).
21. V. S. Volkov, S. I. Bozhevolnyi, S. G. Rodrigo, L. Martín-Moreno, F. J. García-Vidal, E. Devaux, and T. W. Ebbesen, "Nanofocusing with channel plasmon polaritons," Nano Lett. **9**(3), 1278–1282 (2009).
22. S. I. Bozhevolnyi, V. S. Volkov, E. Devaux, J.-Y. Laluet, and T. W. Ebbesen, "Channel plasmon subwavelength waveguide components including interferometers and ring resonators," Nature **440**(7083), 508–511 (2006).
23. V. S. Volkov, S. I. Bozhevolnyi, E. Devaux, J.-Y. Laluet, and T. W. Ebbesen, "Wavelength selective nanophotonic components utilizing channel plasmon polaritons," Nano Lett. **7**(4), 880–884 (2007).
24. V. A. Zenin, V. S. Volkov, Z. Han, S. I. Bozhevolnyi, E. Devaux, and T. W. Ebbesen, "Dispersion of strongly confined channel plasmon polariton modes," J. Opt. Soc. Am. B **28**(7), 1596–1602 (2011).
25. D. Arbel and M. Orenstein, "Plasmonic modes in W-shaped metal-coated silicon grooves," Opt. Express **16**(5), 3114–3119 (2008).
26. Y. Li and X. Zhang, "Directional couplers using V-groove plasma waveguides," in *IEEE Symposium on Photonics and Optoelectronics* (Institute of Electrical and Electronics Engineers, New York, 2009), 1–3.
27. R. F. Oulton, G. Bartal, D. F. P. Pile, and X. Zhang, "Confinement and propagation characteristics of subwavelength plasmonic modes," New J. Phys. **10**(10), 105018 (2008).
28. V. S. Volkov, S. I. Bozhevolnyi, E. Devaux, and T. W. Ebbesen, "Compact gradual bends for channel plasmon polaritons," Opt. Express **14**(10), 4494–4503 (2006).
29. E. Palik and G. Ghosh, *Handbook of Optical Constants of Solids II* (Academic Press, 1991).
30. E. Moreno, F. J. Garcia-Vidal, S. G. Rodrigo, L. Martin-Moreno, and S. I. Bozhevolnyi, "Channel plasmon-polaritons: modal shape, dispersion, and losses," Opt. Lett. **31**(23), 3447–3449 (2006).
31. S. I. Bozhevolnyi and J. Jung, "Scaling for gap plasmon based waveguides," Opt. Express **16**(4), 2676–2684 (2008).

1. Introduction

Surface plasmon polaritons (SPPs) are electromagnetic excitations (i.e., combined oscillations of the electromagnetic field and the surface charges of the metal) existing on a metal dielectric interface [1]. Their field distribution is evanescent in the direction perpendicular to the propagation direction, resulting in intense fields that decay exponentially into both (metal and dielectric) media that bound the interface [2]. Over the last decades, there has been a significant advance in SPPs investigations and a number of theoretical [2–4] and experimental [5–7] studies have been reported. Thus, it is expected that SPPs can be advantageously used for creating a new generation of nanophotonics devices and circuits [8, 9]. The main issue in this context is to strongly confine the SPP field in the cross-section (perpendicular to propagation direction), while keeping low propagation losses [10]. It has been shown that nanometer-sized silver nanowires can support strongly confined SPP modes propagating through only 10 μm [11]. Similar properties were expected [12] and indeed found [13] for the electromagnetic excitations supported by chains of metal nanoparticles. Other configurations, including (among others) SPP propagation along metal stripes [14,15], narrow dielectric ridges deposited on metal films [16] and gap waveguides [17] (based on SPP propagation between two metal surfaces) have been suggested. It should be noted that, in general, the SPP confinement is achieved primarily by decreasing the SPP spatial extent into dielectric, thereby increasing the portion of SPP power being absorbed by metal, so that the choice of optimum guiding configuration is subject to trade-off with many intricate issues yet to be elucidated [10]. One of the most promising approaches for achieving strong lateral confinement of the SPP fields (simultaneously with relatively low propagation loss) is to utilize V-grooves milled in otherwise smooth metal films.

Channel SPP modes, or channel plasmon polaritons (CPPs), where the radiation is concentrated at the bottom of such V-shaped grooves, have been first predicted [18] and then

#162315 - $15.00 USD Received 31 Jan 2012; revised 24 Feb 2012; accepted 24 Feb 2012; published 29 Feb 2012
(C) 2012 OSA

experimentally shown [19] to exhibit useful subwavelength guiding properties. Their unique features of strong SPP mode confinement make it possible to bend (and split) CPP waveguides (CPPWs) formed in the materials with extremely small curvature [20]. CPPs have already been found suitable for realization of many passive photonic devises [19–23], and may find important applications as basic building blocks in ultrahigh-speed all-optical signal processing circuits [8, 9]. Note that even though the dispersion properties of strongly confined CPP modes (propagating at telecom wavelengths) have been recently reported [24], inferring the main CPP characteristics (mode index, width and propagation length), the directional coupling in CPPWs that determines the integration potential of CPPW-based photonic circuits (with respect to the maximum allowed density of non-interacting CPPWs) has so far been paid little attention to [25, 26].

Here, we present the results of our investigations at telecom wavelengths (1425-1630 nm) of directional couplers (DCs) based on CPP modes guided by V-grooves cut in a gold film and separated by different distances. The main goal of our work was to characterize the crosstalk between adjacent CPPWs so as to accurately determine the minimum CPPW separation that can still be tolerated with respect to the incurred crosstalk. In principle, this separation is directly related to the CPP mode confinement [9, 19–24]. It should be borne in mind though, that the mode confinement can be characterized in different ways (especially for plasmonic waveguides) leading to different conclusions about the absolute and relative confinement strengths [27]. For example, one can introduce the average (lateral) width w that can be used to determine the largest bend angle $\theta \sim \lambda/w$ allowed by the acceptable level of bend loss. However, such mode width cannot be applied to determine accurately the minimum separation between neighbor waveguide components since it does not take into account the coupling between modes in adjacent waveguide components. For such purpose the investigation of DCs should provide immediately the value of this minimum separation and, therefore, set the limit on the maximum density of waveguide components.

The remainder of this paper is organized as follows. In Section 2 the investigated sample and the experimental arrangement are described. Section 3 is devoted to the experimental results featuring the scanning near-field optical microscope (SNOM) images of CPP-based DCs and their interpretation. In Section 4 we use finite element method (FEM) implemented in COMSOL for numerical simulations of DCs. Finally, the paper is terminated with our conclusions offered in Section 5.

2. Sample description and experimental setup

The sample contained several DCs with channels made as V-shaped grooves, milled by a focused ion-beam (FIB) in a 2-μm-thick gold layer, deposited on a substrate of fused silica covered with an 80-nm-thick indium-tin-oxide layer [Fig. 1(a)]. For each DC one V-groove (called main in our work) was longer and it started from the edge of the sample, while an adjacent second V-groove went parallel to the first one, starting at the distance of approximately 100 μm from the edge of the sample. Two V-grooves were separated by a distance d (measured at the surface level on SEM images), varied for different DCs from 0.08 to 2 μm, over the length of 40 μm; then they were pulled apart (by the use of the S-bend design that connects two parallel 5-μm-offset waveguides over a distance of 5 μm) to increase the separation between the channels to about 10 μm [Fig. 1(b)]. The intention with using S-bends (characterized by the smallest curvature radius ~2.25 μm [22]) after the coupling region and laterally displacing the output DC channels was to decrease the influence of radiation scattered in the coupling region on the signal detected in the output channels. Also it allowed measuring the output more accurately (since the coupling region was fixed, so the intensity distribution in two channels at the output could be measured over some distance, not at one point). Each V-groove had an angle θ close to 25° and depth H of ~1.4 μm [Fig. 1(c)]. For these parameters only the first (fundamental) CPP mode can be guided in the groove [19].

#162315 - $15.00 USD Received 31 Jan 2012; revised 24 Feb 2012; accepted 24 Feb 2012; published 29 Feb 2012
(C) 2012 OSA

The experimental setup was quite similar to those used in our previous experiments [19–24]. It consisted of a scanning near-field optical microscope (SNOM) with a sharp optical fiber tip used as a probe, in-coupling arrangement with a tapered-lensed fiber used to couple light to CPP by illuminating the open end of V-groove from the edge of the sample, and a positioning system consisting of several stages [Fig. 1(d)]. The radiation (wavelength 1425-1630 nm) was delivered from a tunable laser by the polarization-maintaining single-mode fiber (note that the CPP mode is excited efficiently for TE mode [19], when the electrical field is almost perpendicular to the groove's walls and parallel to the sample surface). The adjustment of the in-coupling fiber at the focal distance of approximately 15 μm [Fig. 1(e)] with respect to the illuminated V-groove channel was accomplished while monitoring the SPP propagation along the sample surface with the help of a far-field microscopy arrangement: 20 × objective, mirror and IR-camera. The track of the propagating radiation (distinguishable for all DCs and wavelengths) featured a gradual decay in visibility along the propagation direction. These far-field observations have also confirmed the expected polarization properties of the guided radiation [19] and demonstrated its (relatively) low dissipation.

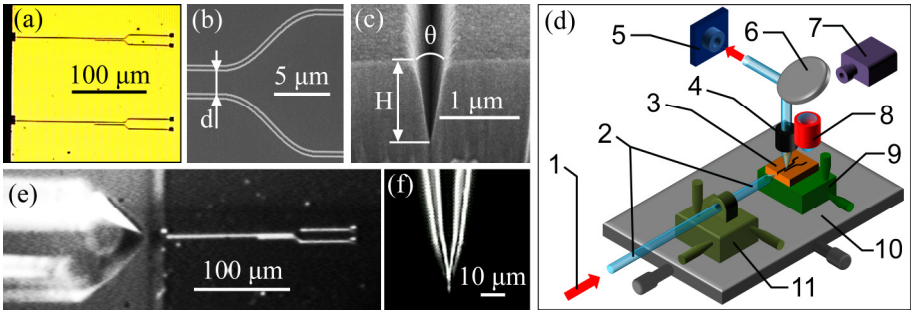

Fig. 1. (a) Microscope image of the sample containing several DCs. (b) SEM image showing the DC with two channels separated by distance d in the coupling region and by approx. 10 μm at the output after two S-bends. (c) SEM image of the cross-section of V-groove reveals groove parameters: angle θ ~25° and depth H ~1.4 μm. (d) Experimental setup: (1) incoming TE-polarized radiation from tunable laser (free-space wavelength 1425-1630 nm); (2) polarization-maintained fiber with a tapered-lensed end used to couple light to CPP mode; (3) sample; (4) SNOM probe with its positioning system; (5) femtowatt InGaAs photoreceiver; (6) mirror; (7) IR camera; (8) 20X objective; (9,10) 2-dimentional X, Y stages; (11) 3-dimentional X, Y, Z stage. (e) In-coupling arrangement with the tapered-lensed fiber in front of the DC input. (f) Microscope image of the uncoated sharpened fiber tip used as a near-field optical probe.

Following these experiments (that include also adjusting the in-coupling fiber position to maximize the coupling efficiency) the whole fiber-sample arrangement was placed under the SNOM head to map the intensity distribution near the sample surface. Tapered fiber tip, used as a SNOM probe, was made from a single-mode silica fiber by ~2 hours etching of a cleaved fiber in 40% hydrofluoric acid with a protective layer of olive oil. The resulting fiber tip had a cone angle of ~30° and curvature radius of less than 100 nm [Fig. 1(f)]. In scanning process the tip was forced to keep the constant distance of a few nanometers from the sample surface by the shear-force feedback. However, inside the V-groove the maximum penetration depth was limited by the shape of the tip. The near-field radiation has been scattered and partially collected by the fiber tip itself, and afterwards guided (in the form of fiber modes) towards the other end of the fiber, where it has been detected by the femtowatt InGaAs photoreceiver (providing both topographical and near-field optical images, simultaneously).

3. Experimental results

3.1 CPP coupling at different wavelengths

We conducted a series of experiments investigating CPP coupling for the DC with the separation distance between V-grooves d = 0.25 μm at different wavelengths varied from

#162315 - $15.00 USD Received 31 Jan 2012; revised 24 Feb 2012; accepted 24 Feb 2012; published 29 Feb 2012
(C) 2012 OSA

1425 nm to 1630 nm (Fig. 2). This DC had the smallest separation between V-grooves (excluding the one with the separation of 0.08 μm, the reason for that will be discussed in Section 3.2), so it was expected to provide the best coupling between CPP modes. It was determined that for the 40-μm-long coupling region the CPP intensity in the main groove evenly decreased, while the CPP intensity in the adjusted groove increased uniformly, reaching roughly the same level as of the first groove CPP intensity. It was difficult to obtain an image with a low background all over the whole coupling region due to short CPP propagation length, so in order to obtain the intensity distribution at the output more precisely, we performed the scanning of the DC by SNOM beyond this coupling region, where the grooves are separated by about 10 μm and no coupling is expected for such large separation [Figs. 2(e)–2(h)]. These measurements confirmed the approximately equal power splitting between output CPPWs for all wavelengths, with some small variations that cannot be ascribed to any simple dependence on the wavelength. These variations could be caused by different contributions of the background, whose level was quite high, as can be seen at the cross-section of optical and topographical images for λ = 1500 nm, averaged along 10 lines (corresponding to the width of 1 μm) perpendicular to the propagation direction [Fig. 2(i)].

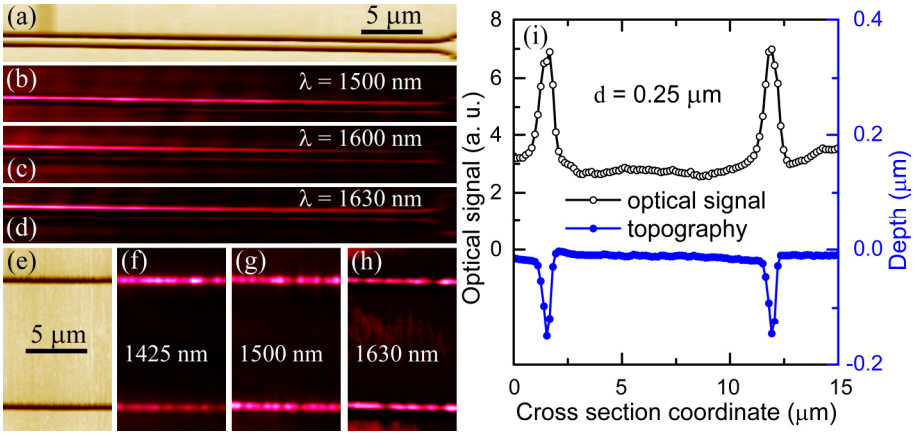

Fig. 2. Experimental results. SNOM (a) topographical and corresponding (b-d) optical images of coupling region for the DC with separation distance d = 0.25 μm, taken at different wavelengths: (b) λ = 1500 nm, (c) λ = 1600 nm, and (d) λ = 1630 nm. SNOM (e) topographical and corresponding (f-h) optical images of output region for the same DC, taken at (f) λ = 1425 nm, (g) λ = 1500 nm, and (h) λ = 1630 nm. (i) Cross-sections of the near-field optical (black hollow circles) and corresponding topographical (blue filled circles) images of (g), averaged along 10 lines perpendicular to the propagation direction.

3.2 CPP coupling for DCs with different separation distances

We carried out another series of experiments investigating CPP coupling at the wavelength of $\lambda \approx$1500 nm for the DCs with channels separation distance varied from 0.08 to 2.0 μm (Fig. 3). Note that for the DC with separation distance of 0.08 μm, as shown on the topographical image [Fig. 3(a)], the middle part between channels is slightly darker than the outside surface, meaning the level of this part is lower than the surface level. Later, it was confirmed with AFM measurements that, for this DC, two V-grooves are overlapped, with the middle part being lower by approximately 150 nm than the surface level. The coupling behavior for such DC is more difficult to understand and compare to other DCs, so that is why it was not chosen for the series with a varied wavelength described in Section 3.2.

#162315 - $15.00 USD Received 31 Jan 2012; revised 24 Feb 2012; accepted 24 Feb 2012; published 29 Feb 2012
(C) 2012 OSA

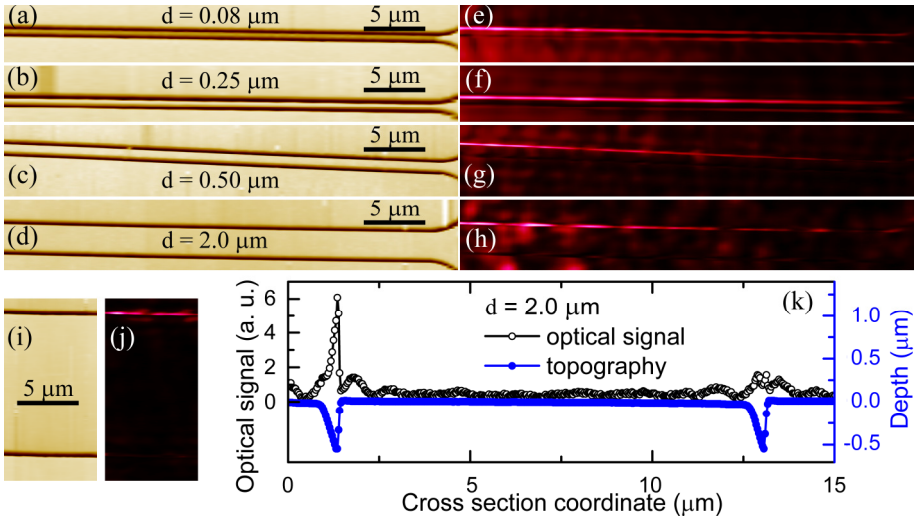

Fig. 3. SNOM (a-d) topographical and corresponding (e-h) optical images of coupling region for the DCs with different separation distances: (a), (e) d = 0.08 μm, (b), (f) d = 0.25 μm, (c), (g) d = 0.50 μm, (d), (h) d = 2.0 μm; taken at the wavelength λ ≈1500 nm. SNOM (i) topographical and corresponding (j) optical images of output region for the DC with separation distance d = 2.0 μm at the same wavelength λ ≈1500 nm. (k) Cross-sections of the near-field optical (black hollow circles) and correspondent topographical (blue filled circles) images of (i), (j), averaged along 5 lines perpendicular to the DC.

Overall, the results showed the following: for the DCs with separation distances of 0.08 and 0.25 μm, the power splitting was approximately equal, while for the DC with the separation distance of 0.50 μm the coupling became weaker, and finally for the DC with the separation distance of 2.0 μm no coupling was observed. In order to be sure that no coupling occurred in the last case (relative to the background), we scanned by SNOM (similar to the case of DC with the separation distance of 0.25 μm described in previous section) the output region of the DC, where two grooves are separated by about 10 μm [Figs. 3(i), 3(j)]. The cross-section of these images, averaged along 5 lines (corresponding to the width of 1 μm) perpendicular to the DC, can be seen in Fig. 3(k). As was expected, the measured optical signal in the adjacent V-groove was at the same level as the background (which is about 6 times smaller than the intensity in the main V-groove); therefore the CPP mode intensity in the adjacent V-groove could not be resolved. Note that the optical signal in the point, corresponding to the deepest part in topography of the adjacent groove, is slightly smaller than the optical signals in nearby points. It could be explained by the enhancement of the background (stray light) at the edges of the groove [28]. This effect is also present for the main grove as a slight variation in the mode profile. However, one can conclude that crosstalk, which could be defined as the ratio of the CPP intensity in the adjacent V-groove to the one in the main groove, is less than 1/6, or approximately −8 dB. It can be compared with the crosstalk of 1 (0 dB), measured for the DC with separation distance of 0.25 μm [see Fig. 2(i)]. It should be noted that the two sets of images (for the DCs with separation distances of 0.25 and 2.0 μm) were made with different SNOM probes (due to its low life-time), which explains the minor differences, such as different background level and different depth of grooves in topography, but it does not influence the crosstalk.

4. Numerical simulation

The directional coupling of CPP modes was investigated numerically by calculating the effective indexes (both real and imaginary parts) of even and odd modes of the double CPPW configuration using the finite-element method (FEM) implemented in the commercial

#162315 - $15.00 USD Received 31 Jan 2012; revised 24 Feb 2012; accepted 24 Feb 2012; published 29 Feb 2012
(C) 2012 OSA

software COMSOL. The simulations were conducted for the wavelength of λ = 1425 nm, 1500 nm, and 1630 nm, with the dielectric permittivity of gold taken from Palik and Ghosh data set [29], and the refractive index of air set to 1. The geometry used in simulations was the following: two V-grooves cut in the gold, each having the width w = 630 nm and depth H = 1420 nm (resulting in the groove angle $\theta \approx 25°$), separated by the distance d (measured at the surface level), which was varied from 40 nm to 3 μm [Fig. 4(a)]. To avoid singularities and the appearance of wedge plasmon polariton (WPP) modes [28, 30], the edges of the grooves and their bottom angles were rounded with curvature radii 50 nm and 10 nm, respectively (later it was confirmed that this rounding does not influence significantly the mode effective index and coupling efficiency, it just removes the local field maxima created by the field enhancement at the sharp edges). The calculated distribution of the horizontal electric field component E_x (which dominates in the dielectric) for the even and odd modes at the wavelength λ = 1500 nm and separation distance d = 0.25 μm are shown in Figs. 4(b), 4(c). Note the sign change of the E_x for the even mode, while it is the same in both V-grooves for the odd mode.

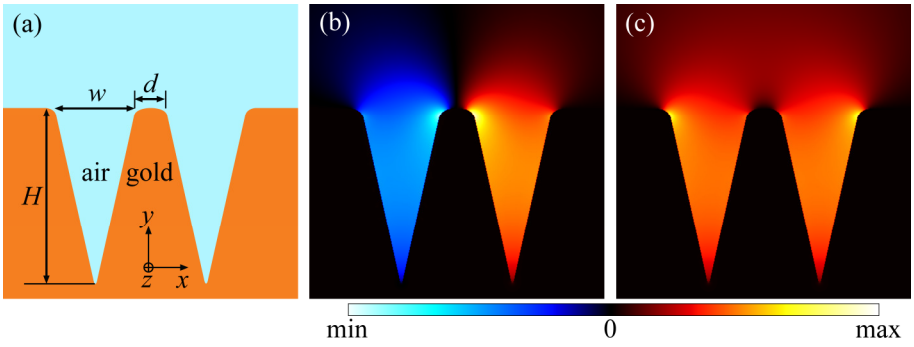

Fig. 4. (a) Coupling configuration used for simulations. Modal structure of (b) even and (c) odd modes represented as the distribution of the dominant electric field component E_x, calculated by the use of the finite-element method (FEM) implemented in the commercial software COMSOL. All panels have a lateral size of 2.5 μm.

Using the aforementioned technique, the odd and even mode effective indexes were calculated for the range of the separation distance d from 40 to 3000 nm at the wavelength λ = 1500 nm. Their real parts, N_{odd} and N_{even}, were compared to the one calculated for the CPP mode in the single groove with the same geometrical dimensions, N_{CPP}, and to the mode effective index of surface plasmon polaritons N_{SPP} [Fig. 5(a)]. Note the large difference between N_{odd} and N_{even} at small separation distances d. This could partially explain the (approximately) equal power splitting observed in the experiment for the DC with separation distance d = 0.25 μm [Fig. 2], since scattering by surface roughness increase rapidly when the mode index approaches the light line. Indeed, the maximum size r_{max} of a scatterer that efficiently scatters the bound waveguide mode into propagating (out of waveguide) waves can be evaluated by the following expression: $\Delta N k_0 r_{max} \sim 2\pi$, where $k_0 = 2\pi/\lambda$, and $\Delta N = N_{mode} - 1$, implying that larger and thereby stronger scatterers start contributing to the mode scattering loss with the decrease of N_{mode}. The even mode, having a considerably smaller effective index, is therefore expected to exhibit significantly stronger scattering losses that might result in its complete attenuation, leaving only the odd mode propagating in a DC and thus resulting in the equal power splitting between two individual CPP modes.

#162315 - $15.00 USD Received 31 Jan 2012; revised 24 Feb 2012; accepted 24 Feb 2012; published 29 Feb 2012
(C) 2012 OSA

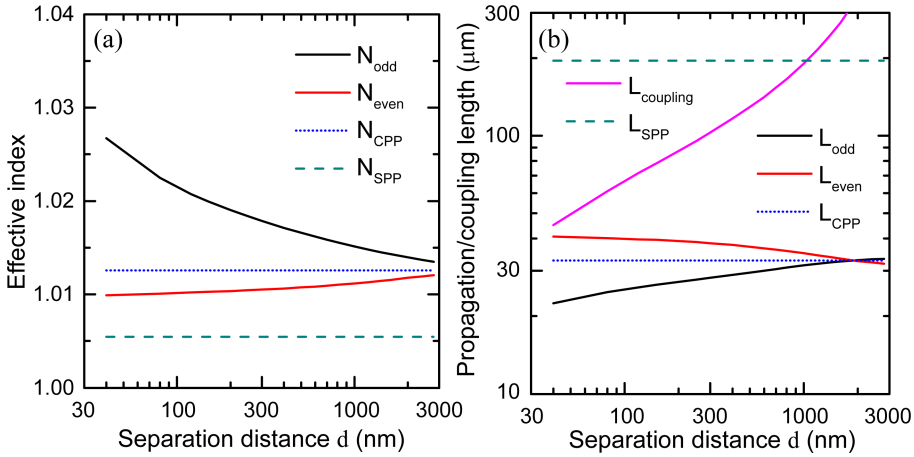

Fig. 5. (a) Effective mode index, calculated for odd (solid black line) and even (solid red line) modes, and compared to the one of CPP (dotted blue line) and SPP (dashed green line) modes, at the wavelength λ = 1500 nm. (b) Propagation length of odd (solid black line) and even (solid red line) modes, compared to the one of CPP (dotted blue line) and SPP (dashed green line) modes, along with the coupling length (solid pink line), at λ = 1500 nm.

The imaginary part of the mode effective index is natural to represent through the mode propagation length: $L = 1/(2\mathrm{Im}[n]k_0) = \lambda/(4\pi\mathrm{Im}[n])$. The propagation lengths of odd and even modes, L_{odd} and L_{even}, were compared to the one calculated for the CPP (L_{CPP}) and SPP (L_{SPP}) modes, along with the coupling length L_{coupling} [Fig. 5(a)]. The coupling length L_{coupling} is the distance (along the DC) between the beginning of the coupling region and the point, where the crosstalk (the ratio of the CPP intensity in the adjacent V-groove to the one in the main groove) is at maxima. The electric field in each groove versus the coordinate z along the propagation direction can be represented as follows:

$$\mathbf{E}_{\mathrm{main}}(x,y,z) = \mathbf{E}_{\mathrm{even}}(x,y)\exp(-in_{\mathrm{even}}k_0 z) + \mathbf{E}_{\mathrm{odd}}(x,y)\exp(-in_{\mathrm{odd}}k_0 z), \qquad (1a)$$

$$\mathbf{E}_{\mathrm{adjacent}}(x,y,z) = \mathbf{E}_{\mathrm{even}}(x,y)\exp(-in_{\mathrm{even}}k_0 z) + \mathbf{E}_{\mathrm{odd}}(x,y)\exp(-in_{\mathrm{odd}}k_0 z), \qquad (1b)$$

where the effective index $n_{\mathrm{even,odd}}$ contains both the real part $N_{\mathrm{even,odd}}$ and the imaginary part responsible for the finite propagation length. In the beginning of the coupling region, at $z = 0$, there is no intensity in the adjacent groove. Assuming the field distribution being mostly the same in magnitude for odd and even mode, $|\mathbf{E}_{\mathrm{even}}(x, y)| \approx |\mathbf{E}_{\mathrm{odd}}(x, y)|$, and taking into account the sign change of dominant field component E_x for the even mode, one can therefore calculate the crosstalk XT as the function of the distance z along the propagation direction:

$$\mathrm{XT}(z) = I_{\mathrm{adjacent}}(z)/I_{\mathrm{main}}(z) = \left|\tan(\Delta n k_0 z)\right|^2, \qquad (2)$$

where $\Delta n = (n_{\mathrm{even}} - n_{\mathrm{odd}})/2$ is the half-difference for the effective indexes of odd and even modes. In order to estimate the coupling length L_{coupling}, one can neglect the imaginary part of Δn (it is a valid assumption, since the propagation length is much larger than the wavelength), so the maximum crosstalk will be at $\Delta n k_0 L_{\mathrm{coupling}} = \pi/2$, or

$$L_{\mathrm{coupling}} = \frac{\lambda}{2(N_{\mathrm{odd}} - N_{\mathrm{even}})}. \qquad (3)$$

Using this equation the coupling length was calculated for the range of separation distances d from 40 to 3000 nm at the wavelength λ = 1500 nm, and compared with the CPP propagation length [Fig. 5(b)]. Note that for the separation distance of 0.25 μm the coupling length is around 90 μm, which is almost twice as long as the 40-μm-long coupling region of

#162315 - $15.00 USD Received 31 Jan 2012; revised 24 Feb 2012; accepted 24 Feb 2012; published 29 Feb 2012
(C) 2012 OSA

the DCs used in our experiment, explaining the observed approximately equal power splitting between two individual CPP modes at the output.

A slight difference between the field magnitude distributions for even and odd modes [Figs. 4(b), 4(c)] caused different propagation lengths for these modes [Fig. 5(b)], especially for small separation distances. As was noted before, when the damping is different for even and odd modes, the maximum crosstalk should be smaller. Indeed, if imaginary part of Δn is non-zero, Eq. (2) can be presented as:

$$\mathrm{XT}(z) = \left|\tan(\{\mathrm{Re}[\Delta n] + i\,\mathrm{Im}[\Delta n]\}\,k_0 z)\right|^2 = \left|\frac{\tan(\mathrm{Re}[\Delta n]k_0 z) + i\tanh(\mathrm{Im}[\Delta n]k_0 z)}{1 + i\tan(\mathrm{Re}[\Delta n]k_0 z)\tanh(\mathrm{Im}[\Delta n]k_0 z)}\right|^2. \quad (4)$$

At coupling distance $z = L_{\mathrm{coupling}}$ calculated by Eq. (3), $\tan(\mathrm{Re}[\Delta n]k_0 z) \to \infty$, so the maximum crosstalk will be:

$$\mathrm{XT}_{\max} = \mathrm{XT}\left(L_{\mathrm{coupling}}\right) = \left\{\tanh(\mathrm{Im}[\Delta n]k_0 L_{\mathrm{coupling}})\right\}^{-2}. \quad (5)$$

Using the relationship between imaginary part of the mode effective index and its propagation length, $L = 1/(2\mathrm{Im}[n]k_0)$, the expression $\mathrm{Im}[\Delta n]k_0$ can be approximated as

$$\mathrm{Im}[\Delta n]k_0 = \frac{n_{\mathrm{even}} - n_{\mathrm{odd}}}{2} = \frac{1}{2}\left(\frac{1}{2L_{\mathrm{even}}} - \frac{1}{2L_{\mathrm{odd}}}\right) = \frac{L_{\mathrm{odd}} - L_{\mathrm{even}}}{4L_{\mathrm{even}}L_{\mathrm{odd}}} \approx \frac{\Delta L}{4L_{\mathrm{CPP}}{}^2}, \quad (6)$$

where $\Delta L = L_{\mathrm{odd}} - L_{\mathrm{even}}$ is the difference in propagation length for even and odd modes. Applying this approximation to Eq. (5), one could finally get the expression for maximum crosstalk:

$$\mathrm{XT}_{\max} = \mathrm{XT}\left(L_{\mathrm{coupling}}\right) = \left\{\tanh\left(\frac{1}{4}\frac{\Delta L}{L_{\mathrm{CPP}}}\frac{L_{\mathrm{coupling}}}{L_{\mathrm{CPP}}}\right)\right\}^{-2}. \quad (7)$$

So it is clear now that the switching effect (when all energy transfers to the adjacent channel, i.e., when the crosstalk is much higher than 1) is limited, since for separation distances such as $L_{\mathrm{coupling}} \le L_{\mathrm{CPP}}$, as followed from Fig. 5(b), $\Delta L \approx L_{\mathrm{CPP}}$, resulting in $\mathrm{XT}_{\max} \approx \{\tanh(1/4)\}^{-2} \approx 16 \approx 12$ dB. Note that for DCs with larger coupling length, when $L_{\mathrm{coupling}} >> L_{\mathrm{CPP}}$, it would be difficult to realize the switching effect practically.

Using the effective mode indexes calculated for the separation distance $d = 0.25$ μm and wavelength $\lambda = 1500$ nm, we compared the expected change of intensities along the propagation direction in the main and adjacent grooves, I_{main} and I_{adjacent}, with the values taken from the experimental data along the coordinate z corresponding to the bottom of each groove with the averaged background being subtracted [Figs. 6(a), 6(b)]. Note that it is difficult to properly take into account the influence of the background since its amplitude and phase inside the groove are unknown. It is seen that the overall behavior of optical signals along the propagation direction is in fair agreement with the conducted simulations. Here one should bear in mind that the intensity of CPP mode (measured by the SNOM) has a strong dependence on the SNOM probe penetration depth inside the V-groove [24, 30, 31]. The later, along with the background level, was used to estimate the uncertainty of experimental data, which can be seen as error bars in Fig. 6(b).

Furthermore, the crosstalk $I_{\mathrm{adjacent}}/I_{\mathrm{main}}$ was calculated for the separation d varied from 40 to 3000 nm, at three different wavelengths: 1425, 1500, and 1630 nm, and at different coordinates: $z = 40$ μm (corresponded to the length of the coupling region for the DCs used in the experiments) and $z = L_{\mathrm{CPP}}$ (varied with the wavelength: $L_{\mathrm{CPP}} = 30$ μm at $\lambda = 1425$ nm, 33 μm at $\lambda = 1500$ nm, and 38 μm at $\lambda = 1630$ nm) [Fig. 6(c)]. As was noted before, the CPP propagation length is an important length parameter for the practical realization of waveguide components, so in order to use wavelength-dependent behavior of DCs (i.e., for switching,

#162315 - $15.00 USD Received 31 Jan 2012; revised 24 Feb 2012; accepted 24 Feb 2012; published 29 Feb 2012
(C) 2012 OSA

modulation, wavelength demultiplexing, and power splitting), one should look for DC configurations that would result in the coupling length being smaller than (or, at least, about) the propagation length L_{CPP}. In addition, the results presented in Fig. 6(c) can be used to evaluate the smallest CPPW separation distance that would result in the crosstalk being below a given limit. For example, if the crosstalk should be less than −10 dB at the wavelength of 1500 nm, then V-grooves should be separated by more than 1 μm. Thus this figure reflects the limit on integration density of considered CPPWs and corresponding waveguide components. Finally, it should be borne in mind that the above results are related to the V-grooves in gold having particular depth of 1.4 μm and groove angle of 25°, so that the CPPW characteristics have to be scaled accordingly when considering other V-groove parameters [30, 31].

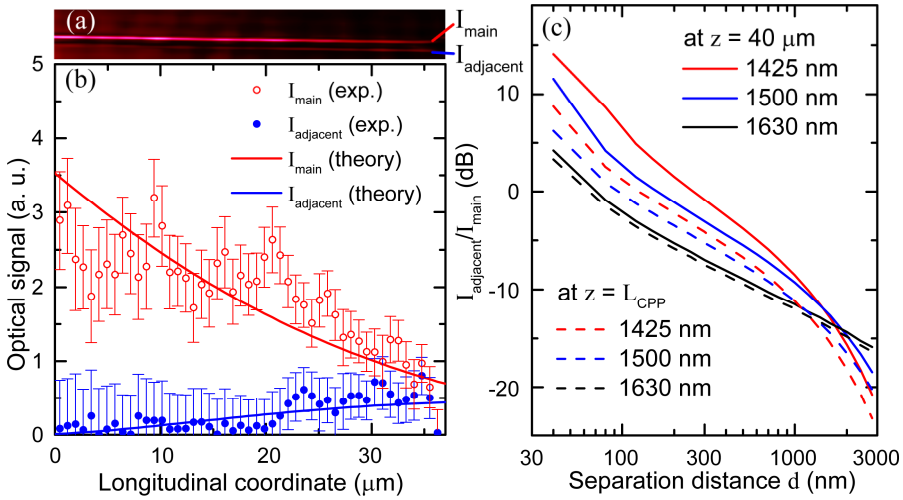

Fig. 6. (a) SNOM optical image of coupling region for the DC with separation distance d = 0.25 μm, taken at the wavelength λ = 1500 nm. (b) Experimental values of the optical signal, varied along the propagation direction, corresponding to optical image (a), calculated inside the main (red hollow circles) and adjacent (blue filled circles) grooves relative to the background, and compared with the results of numerical simulations (red and blue lines for the intensities in the main and adjacent grooves, correspondingly). Error bars are estimated from the maximum variations of the CPP intensity, where we took into account the influence of the background level and the penetration depth of SNOM probe into the groove. (c) Crosstalk $I_{adjacent}/I_{main}$, calculated numerically for separation d varied from 40 to 3000 nm, at different wavelengths: 1425 nm (red lines), 1500 nm (blue lines), and 1630 nm (black lines), and at different longitudinal coordinates: z = 40 μm (solid lines) and $z = L_{CPP}$ (dashed lines).

5. Conclusions

Overall, we studied the directional coupling of CPP modes guided by V-grooves cut in gold film, separated by distance d ≈0.08-2 μm. The experimental observations performed by the use of SNOM showed the strong coupling for d = 0.25 μm (output crosstalk was approximately 0 dB after the 40-μm-long coupling region), independently on the wavelength (over the range 1425-1630 nm). With the increase in separation distance d the output crosstalk decreased, and for d = 2.0 μm no coupling was observed.

In addition to experimental study, we performed numerical simulations based on finite-element method implemented in commercial software COMSOL. For d = 0.25 μm the calculated coupling length was 90 μm (which is almost twice as long as the length of coupling region), explaining approximately equal power splitting obtained in the experiment. Moreover, significantly different propagation losses (related both to different electric field distribution in metal and different effective indexes with corresponding different losses on scattering at surface roughness) for even and odd mode explained the (approximately) equal power splitting for the whole range of wavelengths (1425-1630 nm). On the other hand, the

#162315 - $15.00 USD Received 31 Jan 2012; revised 24 Feb 2012; accepted 24 Feb 2012; published 29 Feb 2012
(C) 2012 OSA

coupling length calculated for the DC with the separation d = 2.0 μm resulted in the output crosstalk of −14 dB, supporting the experimentally obtained data (from which the crosstalk was evaluated to be less than −8 dB).

The results of numerical simulations also provide the important design guidelines for practical realization of both coupling-dependent waveguide components (utilizing DCs for switching, modulation, wavelength demultiplexing, and power splitting), and, oppositely, configurations in which the crosstalk should be avoided. The latter, with the proper criterion, could be treated as the upper limit on the density of CPP-based waveguide components.

Acknowledgments

The authors gratefully acknowledge financial support from the Danish Council for Independent Research (FTP-project no. 09-072949 ANAP) and the European Research Council (ERC) (grant 227577).

#162315 - $15.00 USD Received 31 Jan 2012; revised 24 Feb 2012; accepted 24 Feb 2012; published 29 Feb 2012
(C) 2012 OSA